



This is a repository copy of *Understanding the effects of oxyfuel combustion and furnace scale on biomass ash deposition*.

White Rose Research Online URL for this paper:
<http://eprints.whiterose.ac.uk/143484/>

Version: Accepted Version

Article:

Yang, X., Szuhánszki, J., Tian, Y. et al. (3 more authors) (2019) Understanding the effects of oxyfuel combustion and furnace scale on biomass ash deposition. *Fuel*, 247. pp. 36-46. ISSN 0016-2361

<https://doi.org/10.1016/j.fuel.2019.03.031>

Article available under the terms of the CC-BY-NC-ND licence
(<https://creativecommons.org/licenses/by-nc-nd/4.0/>).

Reuse

This article is distributed under the terms of the Creative Commons Attribution-NonCommercial-NoDerivs (CC BY-NC-ND) licence. This licence only allows you to download this work and share it with others as long as you credit the authors, but you can't change the article in any way or use it commercially. More information and the full terms of the licence here: <https://creativecommons.org/licenses/>

Takedown

If you consider content in White Rose Research Online to be in breach of UK law, please notify us by emailing eprints@whiterose.ac.uk including the URL of the record and the reason for the withdrawal request.



eprints@whiterose.ac.uk
<https://eprints.whiterose.ac.uk/>

Understanding the effects of oxyfuel combustion and furnace scale on biomass ash deposition

Xin Yang ^a, János Szuhánszki ^a, Yufei Tian ^a, Derek Ingham ^a, Lin Ma ^{a,*}, Mohamed Pourkashanian ^a

^a Energy 2050, Department of Mechanical Engineering, University of Sheffield, Sheffield S10 2TN, UK

1 **Abstract**

2 Recycled wood oxyfuel combustion is attractive for the advantages of reusing the waste bioenergy and reducing
3 the carbon emissions. However, the changes in the fuel properties and combustion conditions can lead to uncertainties
4 in the ash deposition. In addition, the understanding of the differences in the ash deposition between the pilot-scale
5 and full-scale furnaces is very limited. We have performed ash deposition experiments on a 250 kW pilot-scale
6 furnace for recycled wood air and oxyfuel combustion along with the EI Cerrejon coal combustion as a reference. A
7 CFD-based ash deposition model, which uses the excess energy based particle sticking model, has been developed
8 and the predictions are in qualitative agreement with the measurement data. The results suggest that, besides furnace
9 temperature, the aerodynamics and ash physicochemical properties dictate the ash deposition. The recycled wood has
10 a much higher deposition rate than the coal in the pilot-scale furnace; however, the biomass can numerically have a
11 lower deposition rate under high velocities close to the full-scale boilers. This is mainly due to the biomass having a
12 much lower sticking efficiency since it has high calcium and silicon concentrations and low potassium concentration.
13 Although the effect of oxyfuel combustion is small and within the experimental uncertainties, it is found that oxyfuel
14 combustion can affect the particle impaction and sticking behaviours depending on the fly ash properties and these
15 effects occur in different ways in the pilot-scale and full-scale conditions. Great care should be taken to perform the
16 transfer of the deposition observations from the pilot scale to the full scale and this is because the furnace scale has
17 an effect on the selective deposition behaviour. In this paper a relationship between the fly ash properties (ash
18 composition, size, etc.) and ash deposition for the woody biomass has been proposed. Additionally, the uncertainty

* Corresponding author.
E-mail address: lin.ma@sheffield.ac.uk.

19 analysis of the CFD modelling is undertaken, which indicates that the fly ash size distribution and the heterogeneity
20 are responsible for the major source of errors along with the experimental uncertainties.

21 **Keywords:** ash deposition, biomass, oxyfuel combustion, CFD, furnace scale, uncertainty analysis.

22 **1 Introduction**

23 Oxyfuel combustion, which replaces the air by the recycled flue gases and high purity oxygen for producing the
24 flue gas with a high CO₂ concentration, is regarded as a promising technology to achieve a near-zero CO₂ emission
25 in both existing and new power stations [1]. By firing biomass, which is often regarded as a low carbon energy,
26 oxyfuel combustion has the potential to achieve negative net CO₂ emissions. In the UK, taken into consideration the
27 supply chains and the economy, recycled wood is a potential biomass source for power generation due to its
28 indigenous availability and low cost. Therefore, recycled wood oxyfuel combustion is an attractive approach to
29 remove CO₂ from the atmosphere and help to meet the stringent carbon budgets of the UK [2], which aims to cut
30 greenhouse gas emissions by at least 80% of the 1990 levels by 2050. Due to the changes in the fuel properties of
31 biomass and oxyfuel combustion conditions, many researches have been undertaken in order to study combustion
32 (ignition and flame stability), radiation heat transfer, and pollutant emissions. It is regarded that it is technically
33 feasible to achieve the flame stability and retrofit the heat transfer for biomass oxyfuel combustion through the
34 adjustment of the oxygen inlet concentration and the recycled flue gas ratio [3-5]. The other technique issues could
35 result from the ash deposition and this is due to the changes in the combustion conditions and the physicochemical
36 properties in the recycled wood. All the changes can cause uncertainties in the ash deposition, which is a significant
37 factor in the design and operation of utility boilers. Therefore, this study focuses on studying the ash deposit formation
38 for recycled wood oxyfuel combustion.

39 First, it is important to understand how the oxyfuel combustion condition can affect the ash deposit formation.
40 Fryda et al. [6, 7] experimentally investigated the ash deposit formation for coal combustion and coal-biomass co-
41 combustion under oxyfuel conditions (30 vol% O₂) in a drop tube furnace. Similar temperature and velocity profiles
42 were designed for both the air and oxyfuel combustion conditions. The results obtained show that the ash deposition
43 rates were higher under oxyfuel conditions and the differences were mainly as a result of the changes in the physical
44 properties of the flue gas (higher CO₂ concentration, higher gas density, etc.). The slight shift in the bulk fly ash size
45 to being coarser was observed for one of the cases investigated, and this could also be responsible for the increase in
46 the ash deposition rate. Also, Yu et al. [8] experimentally found that there was a higher ash deposition rate under
47 oxyfuel combustion conditions (27 and 32 vol% O₂) than air combustion for two US bituminous coals combusted in

48 a 100 kW down-fired furnace. The authors proposed that the differences were mainly due to the aerodynamic changes
49 in the gas flow (lower gas velocity) and combustion temperatures, rather than the changes in the chemistry of the ash
50 particles. However, Li et al. [9] experimentally found lower ash deposition rates under oxyfuel combustion conditions
51 (30 vol% O₂) for a Chinese bituminous coal in a 25 kW down-fired furnace. They suggested that the lower particle
52 Stokes numbers, which were due to the lower furnace velocity and slightly smaller particle size under oxyfuel
53 combustion conditions, were responsible for the changes in the ash deposition rate. The authors proposed that the ash
54 chemistry of the deposits was basically not changed, which was not responsible for the differences in the ash
55 deposition rate. Another different experimental investigation was carried out by Brink et al. [10] and Jurado et al.
56 [11] for coal/biomass oxyfuel combustion/co-combustion with the flue gas recirculation in down-fired furnaces (300
57 kW and 100 kW, respectively). They found that the ash deposition under oxyfuel combustion was basically similar
58 to air combustion based on the SEM images of the deposits, the deposit chemistry and the visual observations of the
59 deposit build-up. The discrepancies in the effect of oxyfuel combustion on the ash deposit formation can be found in
60 these experimental findings and it can be concluded that: (i) the effects mainly result from the aerodynamic changes
61 in the small scale furnaces, rather than the chemical changes in the fly ash/deposit [6-9]; (ii) the effect of the oxyfuel
62 combustion condition on the fly ash formation could be decreased when the flame temperature/char temperature are
63 close to those in the air combustion [12]. Therefore, it is important to undertake a CFD analysis on the effect of the
64 aerodynamics on the ash deposition in order to understand the detailed effect of oxyfuel combustion on the particle
65 impaction and sticking behaviours.

66 Second, it is important to understand how the physical and chemical changes of biomass can affect the ash deposit
67 formation. On the one hand, the pulverised recycled wood particles used for power generation generally have much
68 larger particle sizes than the pulverised coal particles. Particles with a higher particle size could increase the particle
69 impaction efficiency, but can also reduce its sticking efficiency due to the increase in the particle kinetic energy. The
70 overall effect of particle size on ash deposit formation is dependent on the furnace velocity conditions, where coarser
71 particles might be easier to deposit under the low velocity conditions in small scale furnace [13]. On the other hand,
72 the pulverised wood particles might have irregular shapes than the spherical shape, which might affect the combustion
73 behaviour and the particle trajectories. For ash deposit formation in the post-combustion region, the effect of ash
74 particle shape on ash deposition could be alleviated for the ash particles with the melting history due to the increased
75 spherical shape after melting [14]. Amand et al. [15] reported the experimental studies of ash deposit formation for
76 a demolition wood combustion in a 12-MWth circulating fluidized-bed (CFB) boiler. They found that KCl was
77 responsible for the serious ash deposition problem while the contamination of Zn (zinc) without chlorine cannot

78 cause a serious ash deposition problem. In this study, the recycled wood have high calcium and silicon concentrations
79 and low potassium/chlorine concentration in the fuel. This suggests that the recycled wood ash belongs to the ash
80 type with less ash deposition issues than the ash types with the high potassium level according to the ash classification
81 method proposed by Vassilev et al. [16, 17], which is based on the relationship between the ash fusion behaviour and
82 ash composition. In addition, a similar method proposed by Nazelius et al. [18] indicates that this kind of ash type
83 belongs to the low-medium slagging ash for the fixed bed combustion condition. However, under the pulverised fuel
84 combustion condition, in addition to the overall ash fusion behaviour, the ash deposit formation is dictated by the
85 particle size based on the ash chemistry, physical property (size, density, etc.), and furnace operation conditions
86 (temperature and velocity). These factors lead to uncertainties when only using the ash fusion behaviour based on
87 the bulk ash composition to predict the ash deposition for the pulverised fuel combustion condition.

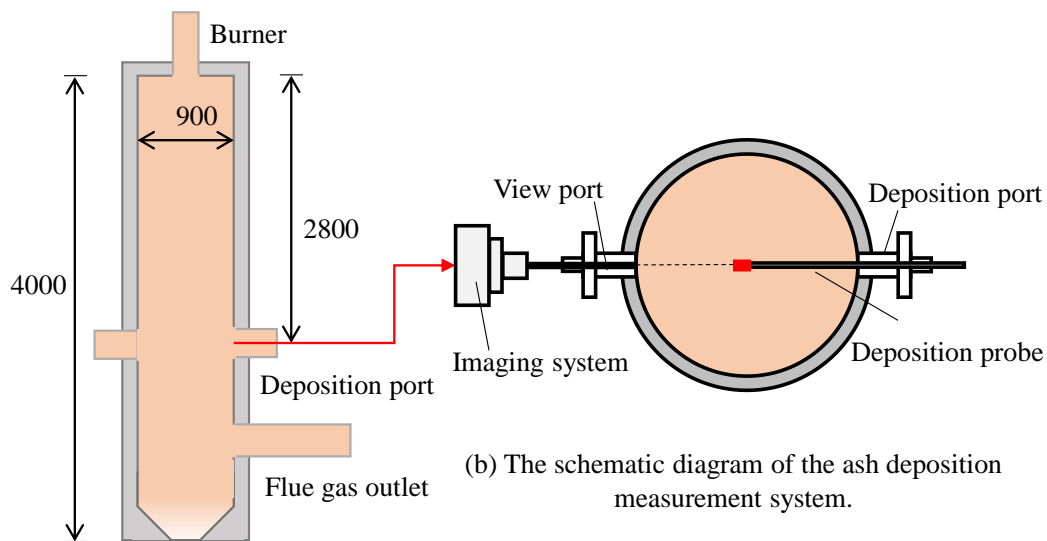
88 Third, it is important to transfer the knowledge of the ash deposition observations in the lab/pilot-scale furnaces
89 into full-scale boilers. To the authors' knowledge, most studies in ash deposit formation for the pulverised fuel
90 oxyfuel combustion were conducted in lab/pilot-scale furnaces and there has been little modelling/experimental work
91 on the ash deposition of oxyfuel combustion under different scaled furnace conditions, especially between the pilot-
92 scale furnaces and the full-scale boilers. Although the smaller scaled furnaces are designed to match the time-
93 temperature history of the particles within the full-scale boilers, the furnace velocity condition is much lower under
94 the smaller scaled furnaces, which can affect the particle impaction and sticking behaviours. Therefore, for practical
95 reasons, it is significant to understand the difference in the ash deposit formation under the oxyfuel combustion
96 among the different scaled furnace conditions.

97 This paper aims to experimentally and numerically investigate the ash deposit formation for the recycled wood
98 under air combustion and oxyfuel combustion conditions along with the EI Cerrejon coal air combustion as a
99 reference. First, the three ash deposition cases have been experimentally conducted in the pilot-scale PACT 250 kW
100 air/oxyfuel combustion test facility (CTF). Second, the ash deposition models based on CFD analysis have been
101 developed and validated against the experimental data. Also, the initial modelling uncertainties have been analysed
102 in order to better understand the modelling conclusions. Third, through the developed ash deposition models, the
103 effect of oxyfuel combustion conditions (the O₂ concentration) and the influence of the different scaled furnace
104 velocity conditions on ash deposition are studied. In addition, the practical implications from transferring the
105 deposition observations in the pilot-scale furnace to full-scale boiler are discussed.

106 **2 Experimental data**

107 **2.1 Pilot-scale furnace and combustion tests**

108 The PACT 250 kW air/oxy-fuel combustion test facility (CTF) is a single-burner down-fired cylindrical furnace,
 109 which has an overall length of 4 m and an inner diameter of 0.9 m, as show in Figure 1 (a). Two different scaled
 110 versions of commercially available low NO_x burners have been fitted to the furnace. The swirl burner for coal
 111 combustion has been manufactured by Doosan Babcock while the one for biomass combustion has been
 112 manufactured by General Electric. Both burners consist of a primary register through which the pulverized solid fuel
 113 and the primary oxidiser stream at ambient temperatures are fed and the secondary and tertiary registers for delivering
 114 the rest of the preheated oxidizer. The oxidizer flowrate ratio and swirling intensity through the secondary and tertiary
 115 registers in both burners are able to be adjusted in order to produce a stable swirled flame. During the stable operation,
 116 the combustion air flowrate is kept constant in order to achieve a consistent flow field, and the feed rate of the
 117 pulverised solid fuel is adjusted in order to maintain the excess oxygen level in the flue gas of 3.5% (dry basis).



(a) The schematic diagram of the pilot-scale furnace.

(b) The schematic diagram of the ash deposition measurement system.

118

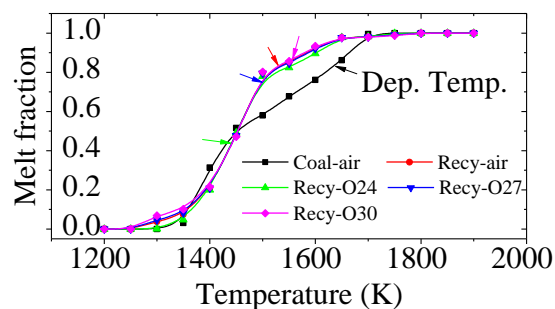
119 **Figure 1 The schematic diagrams of (a) the pilot-scale furnace (mm) and (b) the ash deposition measurement**
 120 **system.**

121 **Table 1 Fuel properties of the EI Cerrejon coal (Coal) and the recycled wood (REC) that were used for the**
 122 **CFD calculations.**

	Coal	REC	as received	Coal	REC
SiO ₂	39.9	44.4	Moist.	7.63	5.8
Al ₂ O ₃	16.6	5.8	Vol.	35.5	73.9
Fe ₂ O ₃	10.8	7.6	FC	54.0	17.1
CaO	14.4	29.5	Ash	2.9	3.2

MgO	1.9	4.1	GCV (kJ/kg)	28.7	18.4
K ₂ O	1.6	2.6	DAF	Coal	REC
Na ₂ O	1.9	1.5	C	80.9	51.9
TiO ₂	0.6	0.9	H	5.12	6.0
P ₂ O ₅	0.8	0.6	N	1.65	0.4
SO ₃	11.4	3.0	O	11.8	41.7

123 Table 1 shows the properties of the EI Cerrejon coal and the recycled wood, including the proximate and ultimate
124 analysis, as well as the major ash composition. As expected, the biomass has a much higher volatile and lower fixed
125 carbon than the coal. Also, the biomass has a much higher oxygen concentration than the coal. Therefore, a much
126 higher concentration of oxygen and lower concentration of carbon in the fuel give rise to a much lower heating value
127 for the biomass than the coal. Both fuels have relatively low ash content of approximately 3%. With regard to the
128 ash composition, the coal is mainly composed of silicon, alumina, calcium, sulphur and iron relevant phases whereas
129 the recycled woody biomass is mainly composed of silicon and calcium relevant phases. Figure 2 shows the melting
130 behaviours of these two fuels under different combustion conditions based on the bulk ash composition by using the
131 chemical equilibrium software Factsage with the 'SLAGB' database with possible 2-phase immiscibility. Generally,
132 the melting curves are similar between the two fuels although the biomass ash shows a higher melting potential under
133 the temperature range from 1550 K to 1800 K. The effect of oxy-fuel combustion on the melting potential is marginal
134 while the Oxy24 case has a much lower melt fraction compared to the other cases due to the lower furnace
135 temperature. However, it should be noted that the melting behaviours are based on the bulk ash composition. For
136 woody biomass, silicon and calcium may occur in different minerals and solid particles [19], which have much higher
137 melting temperatures than that of the bulk ash composition. Table 2 shows the operating conditions for the three
138 different cases (including one coal air combustion case and two biomass combustion cases for the air and oxyfuel
139 conditions). The oxyfuel case has been tested with a total inlet oxygen concentration of 27% (Oxy27) in order to
140 obtain a similar temperature distribution and radiative heat transfer in the air-fired combustion conditions.



141

142 **Figure 2 The predicted melting curves by using the chemical equilibrium method as a function of the**
143 **temperature for different combustion conditions based on the bulk ash composition: the arrows represent**
144 **the melt fraction under the furnace temperature at the deposition regions.**

145
146

Table 2 Summary of the operation conditions of the pilot-scale furnace that were used for the CFD calculations (Coal-air, REC-air and REC-Oxy27).

	Coal-air	REC-air	REC-O27
Mass flow rate (kg/hr)			
Fuel	25.7	42.1	42.1
Primary	60.1	52	55.7
Secondary	92.2	148	154.7
Tertiary	158.3	88.8	92.8
Inlet gas temperature (K)			
Primary	297	294	296
Secondary	525	524	525
Tertiary	525	524	525
Oxygen concentration (vol.%)			
Primary	20.84	20.92	21.09
Secondary	20.84	20.92	28.30
Tertiary	20.84	20.92	28.30

147 2.2 Ash deposition measurements

148 Figure 1 (b) shows a schematic diagram of the ash deposition measurement system, which consists of the deposit
149 sampling system and the imaging system. The deposit sampling system consists of the ash deposition probe with a
150 detachable uncooled ceramic coupon at the tip in order to collect the deposits. To simulate the temperature condition
151 for the slagging formation on a radiant superheater tube in the utility boilers, the ash deposition probe is inserted into
152 the middle of the cross section of the furnace, which is located at the downstream of the combustion chamber with a
153 distance of 2.8 m from the top wall of the furnace. The imaging system is used to record the deposit growth and the
154 shedding. Much care needs to be taken to choose the outer diameter of the deposit sampling coupon. Ideally, through
155 choosing a proper outer diameter, it is possible to match the particle Stokes number ($St = (\rho_p d_p^2 \bar{U}) / (9\mu_g D)$) with
156 the one in utility boilers in order to maintain a similar particle impaction behaviour. However, due to the much lower
157 velocity condition in the pilot-scale furnace (0.5 m/s) than in the utility boilers (10–25 m/s), the outer diameter should
158 be scaled to be 1/20-1/50 of the dimension of a real superheater tube, which is difficult to be manufactured and used
159 for collecting the ash deposition for the pilot-scale furnace. Therefore, in this study, a typical dimension of the real
160 superheater tube of 37 mm is used. This indicates that the dimension leads to the particle Stokes number to be 1/20-
161 1/50 of the one in the real boilers, which can greatly reduce the impaction efficiency of small particles. To the author's
162 knowledge, the only available research where the particle Stokes numbers have been matched is the ash deposition
163 experiments undertaken in the Sandia National Laboratories Multifuel Combustor (30 kW) [20], which is able to be
164 operated under a much higher furnace velocity of 5 m/s. However, it should be noted that, in addition to particle

165 impaction, the particle sticking behaviours are dictated by the particle kinetic energy ($\frac{\pi}{12}\rho_p d_p^3 V_p^2$). Therefore, the
166 ash deposit formation in the lab/pilot scale furnaces could be different from the real boilers and this is due to the
167 much lower particle Stokes number and particle kinetic energy.

168 The ash deposition rate is characterised by the ratio of the deposit mass to the deposition time. The deposition
169 time of four/six hours is used in order to ensure that enough deposits are collected before the shedding occurs. The
170 experimental uncertainties for the ash deposition rate mainly result from the repeatability error and the variability in
171 the fuel feed rate and fuel properties (ash content, ash composition, etc.). The repeat ash deposition experiments of
172 coal combustion have been undertaken twice. The relative variability (represented by the ratio of the standard
173 deviation to the averaged value of the deposition rate) in the twice-repeated ash deposition experiments of coal
174 combustion is approximately 12%. Since the biomass combustion has a much higher ash deposition rate than the coal
175 combustion, this could help to reduce the variability [20]. Therefore, it is assumed that the relative variability for
176 biomass combustion is not higher than coal combustion and the repeated experiments of biomass combustion are not
177 undertaken for the reason of the experimental expense. The relative variability in the fuel feed rates are within 5% in
178 order to maintain the excess oxygen level in the flue gas of 3.5% (dry basis). Due to the relatively low ash content,
179 the relative variabilities of the ash content have large values of 29% and 34% for coal and biomass, respectively. The
180 relative variabilities of the major ash composition (represented by SiO₂, CaO, Al₂O₃, Fe₂O₃, etc.) are within
181 approximately 10%, which may not greatly affect the ash composition. Also, the relative variabilities of the averaged
182 diameter of the particle size distribution are within a small value of 3%. Therefore, only the variabilities in the
183 repeatability error and the ash content have been taken into account in this study, which results in the combined
184 standard uncertainties (represented by the root sum of the squares of the two relative variabilities [21]) in the ash
185 deposition rate of 32% and 35% for coal combustion and biomass combustion, respectively.

186 **3 Mathematical models**

187 **3.1 Combustion modeling**

188 Pulverized fuel combustion is modeled by Euler–Lagrange approaches through three-dimensional (3D) CFD-
189 based mathematical models. Mathematical submodels, such as the Reynolds Stress model (RSM), Discrete Ordinate
190 model (DOM), the eddy-dissipation model (EDM) and Discrete Phase Model (DPM), are used for modelling the
191 turbulence, radiation heat transfer, gas combustion, and particle trajectories, respectively. The combustion of the
192 solid fuel particles can be modelled by the sequential processes of inert heating, moisture release, devolatilisation,
193 char combustion, and finally inert heating/cooling of ash particles. In order to take into account the high concentration

194 of CO₂ under oxy-fuel conditions, the in-house developed radiation property models (the full-spectrum correlated k
 195 (FSCK) model and Mie theory based data) are used [22-24]. The previous studies have shown a relatively hotter
 196 flame after using the refined radiation property models while the effect on the temperature at the downstream of
 197 furnace is small [23]. In addition, reasonable agreements have been obtained between the experimental data and the
 198 predicted results for the in-flame gas species, the flue gas species and the surface incident radiation on the furnace
 199 walls. More details of the 3D CFD combustion models may be found from our previous work [23, 25, 26].

200 It should be noted that the particle combustion models are not directly developed for ash deposition prediction.
 201 In this study, since the deposit formation is relevant to the post-combustion region, the formation of ash particles are
 202 predicted by the original coal particle size distribution and the ash content [27] while the density of the ash particles
 203 are predicted by employing the original ash composition. The fly ash formation routes (including fragmentations of
 204 coal/char/excluded minerals, coalescence of included minerals, and vaporization/agglomeration/condensation of
 205 salts/organic-bound inorganics [28, 29]) are often neglected in the particle combustion modelling due to the
 206 complexity. Up to date, it is still a challenge to directly incorporate the detailed fly ash formation models into the
 207 CFD based combustion modelling [29, 30]. However, this limitation can lead to the uncertainties in the
 208 physicochemical properties (ash composition, size, density, etc.) of the fly ash particles, which are among the key
 209 factors in dictating the ash deposit formation. More details of the uncertainty analysis of the effect of fly ash formation
 210 on ash deposition are discussed in the next section.

211 3.2 Ash deposition models

212 The trajectories of the coal particles are modelled in a Lagrangian reference frame by using the DPM. They are
 213 governed by the particle motion equation, which is a balance of the drag, gravity, and other body forces as formulated
 214 in the equation [31]:

$$m_p \frac{d\vec{v}_p}{dt} = m_p \left(\frac{18\mu_g C_D Re_p}{\rho_p d_p^2} (\vec{v}_g - \vec{v}_p) + \frac{\vec{g}(\rho_p - \rho_g)}{\rho_p} \right) + \vec{F} \quad (1)$$

215 where, \vec{v} , ρ , μ and d are the velocity, density, viscosity and diameter of the particles, respectively; the subscripts p
 216 and g refer to the particle and gas, respectively, C_D is the drag coefficient, and \vec{F} is the other body forces, such as the
 217 thermophoretic force, etc. In the deposition experiments, there is no initial deposition layer with fine particles and
 218 the leeward section of the uncooled deposition tube is clean. Hence, it is reasonable to neglect the thermophoretic
 219 force for the uncooled probe in this study. The effect of fluid turbulence on the particle trajectories (or termed as the
 220 turbulent diffusion) has been considered by the Discrete Random Walk (DRW) model, which integrates the particle
 221 motion equation of a sufficient number of particles using the instantaneous fluid velocity. For the pilot-scale cases,

222 due to the low $Re ((\rho_g \bar{U}_g D_{probe})/\mu_g \approx 70-80)$ in the downstream region and the particle turbulent diffusion is not
 223 considered. In order to resolve the boundary layer, the enhanced wall treatment is enabled. If the near-wall mesh is
 224 fine enough to be able to resolve the fluid viscous sublayer ($y^+ \approx 1$), then the enhanced wall treatment can be
 225 similar to the traditional two-layer zonal model [32].

226 After the arrival rate of the ash particles, $A_{arrival}$, is predicted by the models mentioned above, and it is required
 227 to incorporate a particle sticking model in order to predict the sticking efficiency of particles, E_{stick} . Then the ash
 228 deposition rate can be determined by the product of the arrival rate and the particle sticking efficiency. In this study,
 229 the in-house developed particle sticking model, based on the energy conservation analysis, is used [13], and this has
 230 been validated by the particle sticking behaviours for particles with Stokes number up to approximately seven
 231 (comparable to the particle Stokes number in a full scale furnace) and the ash deposition formation from coal
 232 combustion in a down-fired furnace for particles with a relatively small Stokes number. The sticking model takes
 233 into account the particle properties relevant to the ash chemistry, particle kinetic energy and furnace operation
 234 conditions and considers the partial sticking behaviour and the deposit layer. The particle sticking efficiency, E_{stick} ,
 235 can be determined by the following formula:

$$E_{stick} = \begin{cases} 1, & \text{if } E^* \leq 0 \\ e^{(-9.21 * E^*(1 - f_{melt}))}, & \text{if } E^* > 0 \end{cases} \quad (2)$$

$$E^* = \frac{1}{4} d_m^2 (1 - \cos\theta) + \frac{2}{3d_m} - 0.00536 * d_m^{4.70} * (1 - \cos\theta)^{0.591} - 1 \quad (3)$$

$$d_m = 1 + 0.259 * We^{0.317} \quad (4)$$

236 where, E^* is the excess energy normalized by the surface energy, f_{melt} is the liquid phase content (or termed as the
 237 melt fraction) of the deposit surface, which was estimated by the deposit composition and temperature through the
 238 chemical equilibrium method; d_m is the maximum spread ratio, θ is the contact angle, $We = (\rho_p U_p^2 D_0)/\gamma_{LV}$ is the
 239 particle Weber number, ρ_p is the particle density, U_p is the normal component of the particle impact velocity, D_0 is
 240 the particle diameter and γ_{LV} is the liquid-vapour surface tension.

241 It is necessary to clarify how the parameters in the particle sticking model have been determined in this study.
 242 The ash particle diameter is estimated from the original coal particle size distribution and the ash content as mentioned
 243 earlier. The ash particle density and the liquid-vapour surface tension is estimated by the bulk ash composition [33].
 244 Due to the difficulty in directly considering the viscous effect on the ash particle sticking behaviour, it is indirectly
 245 considered by the wetting behaviour [13]. The f_{melt} is determined by the melt fraction as mentioned in Equation (2).
 246 Then, the contact angle is determined by matching the predicted results with the experimental data in the ash

247 deposition rate. For the coal ash deposition case, the contact angle of 160° is used when the predicted liquid phase
248 content of the deposit surface chemical equilibrium was 83%, which is employed as the value of f_{melt} in this model.
249 For the biomass air combustion case, the same contact angle of 160° is used due to the similar melting curves between
250 the biomass and coal ashes. However, the f_{melt} with a value of 41.5% is half of the predicted liquid phase content in
251 order to match the predicted results with the experimental data. This can be due to the high concentrations in the
252 silicon and calcium and the low potassium concentration in the woody biomass ash and its heterogeneity. For the
253 biomass oxyfuel combustion case, the same assumption is employed as in the biomass air combustion case. The
254 normal component of the particle impact velocity is directly obtained from the CFD modelling analysis. The detailed
255 values of these parameters can be found in the Supplementary Materials.

256 3.3 Case set-up and uncertainty analysis

257 The ‘steady state’ assumptions of the deposition rates are employed to develop the ash deposition sub-models.
258 This is because the thermal boundary is relatively stable for the uncooled tube and the deposit height is within 2mm,
259 which is much smaller compared to the outer diameter (37 mm) of the tube. This does not greatly change the geometry
260 of the deposit surface and affect the particle impaction and deposition behaviour. Kupka et al. [34] experimentally
261 found a linear ash deposition rate in the early stage, which also supports the ‘steady state’ assumption in this study.
262 The two-dimensional (2D) mesh is used as the focus of this study is on the ash deposition formed by the inertial
263 impaction at the windward section of the uncooled tube while 3D can have an effect on the fume ash deposition at
264 the leeward section [35]. The 2D geometry is 0.9m*0.9m with a deposition tube of outer diameter 37mm placed in
265 the central region while the boundary conditions are determined from the combustion cases (temperature, gas species,
266 velocity, ash particle flow rates, etc.). In order to resolve the flow-field within the boundary layer near the deposition
267 surface, Weber et al. [36] suggested the employment of at least twelve grid nodes within the δ_{99} thickness (represented
268 by the boundary layer thickness where the velocity reaches 99% of the free stream velocity) when a first-order
269 numerical scheme is used while Haugen et al. [37] and Bouhairie et al. [38] employed approximately three nodes to
270 be located within the boundary layer by using a higher-order discretization scheme. In this study, the second-order
271 discretization scheme is enabled and the first node is placed at approximately 0.2 mm from the tube which meets the
272 mesh requirement proposed by Weber et al. [36] for the deposition cases in the pilot scale furnace. An additional
273 mesh with the first node displacement of 0.05 mm is tested for the higher velocity case (25 m/s) and the difference
274 in the particle arrival rate is marginal compared to the current mesh. Therefore, in order to reduce the computational
275 resource, the same mesh (0.2 mm) has been used for the higher velocity conditions as well, which meets the criteria
276 used by Haugen et al. [37] and Bouhairie et al. [38]. The averaged y-plus at the deposition tube are 0.05 and 0.74 for

277 the low velocity condition (approximately 0.5 m/s) and high velocity condition (25 m/s), respectively. Again, this
278 indicates that the current boundary mesh should basically meet the requirement for the enhanced wall treatment.
279 More details of the geometry and mesh can be found in the Supplementary Materials.

280 The uncertainty analysis in the CFD modelling is significant in order to understand whether the simulation
281 conclusions are reasonable. In this study, for the CFD modelling of the ash deposition in the post-combustion region,
282 the source of errors in the modelling can come from (i) the experimental measurements, (ii) the numerical parameters
283 and (iii) the model parameters. As mentioned in Section 2.2, for the experimental measurements, the ash content is
284 the major source of error, being 29% and 34% for coal and biomass, respectively. For the numerical parameters,
285 mesh resolution and quality, and the discretization scheme could be the major source of errors. However, these
286 numerical error sources are neglected in this study since a fine mesh with a high quality is used and the second-order
287 discretization scheme are enabled. For the model parameters, the error sources could be generated by the viscous
288 turbulence model, the radiation model and the parameters employed in the ash deposition model. Sensitivity analyses
289 of different viscous models (including the standard k-epsilon, realizable k-epsilon, k-omega SST and Reynolds stress
290 model)¹ and two different types of radiation property models (the in-house developed radiation property model and
291 the traditional radiation property model) have been carried out. The effects of both turbulence models and radiation
292 property models are marginal. Hence, the study neglects the uncertainties in the viscous models and radiation property
293 model since their errors are small compared to other source of errors. However, for fume particle deposition, the
294 uncertainties in the transient modelling (URANS, LES, etc.) of particle-laden flow should be taken into account. For
295 the model parameters, the number of particle size intervals and number of tries in the DRW model could affect the
296 particle arrival rate. The fluctuations in the predicted arrival rate can be minimized by increasing the number of
297 particle size intervals and number of tries. In this study, 50 intervals and 10 tries are used, which results in the relative
298 variability in the deposition rate within approximately 2%. Another major contribution in the error source is generated
299 by the fly ash properties. The first one is the particle size distribution. Becknman et al. [39] measured the particle
300 size of the original coal particles and the bulk fly ash particles, where the fly ash particles showed 7% higher averaged
301 size and 28% lower spreading factor of the Rosin-Rammler distribution than the predicted values by using the current
302 assumption in this study. This represents that the current assumption under predicts the particle size distribution in
303 the coarse and fine ranges, which correspondingly over predicts the distribution in the medium particle range. This
304 is because the detailed fly ash formation mechanisms are not considered in the current assumptions. Therefore, the

¹ Note: For the pilot-scale cases, the laminar model is used due to the low Re ($\approx 70-80$); while the turbulence model is used for high velocity conditions with high Re ($\approx 2300-4300$).

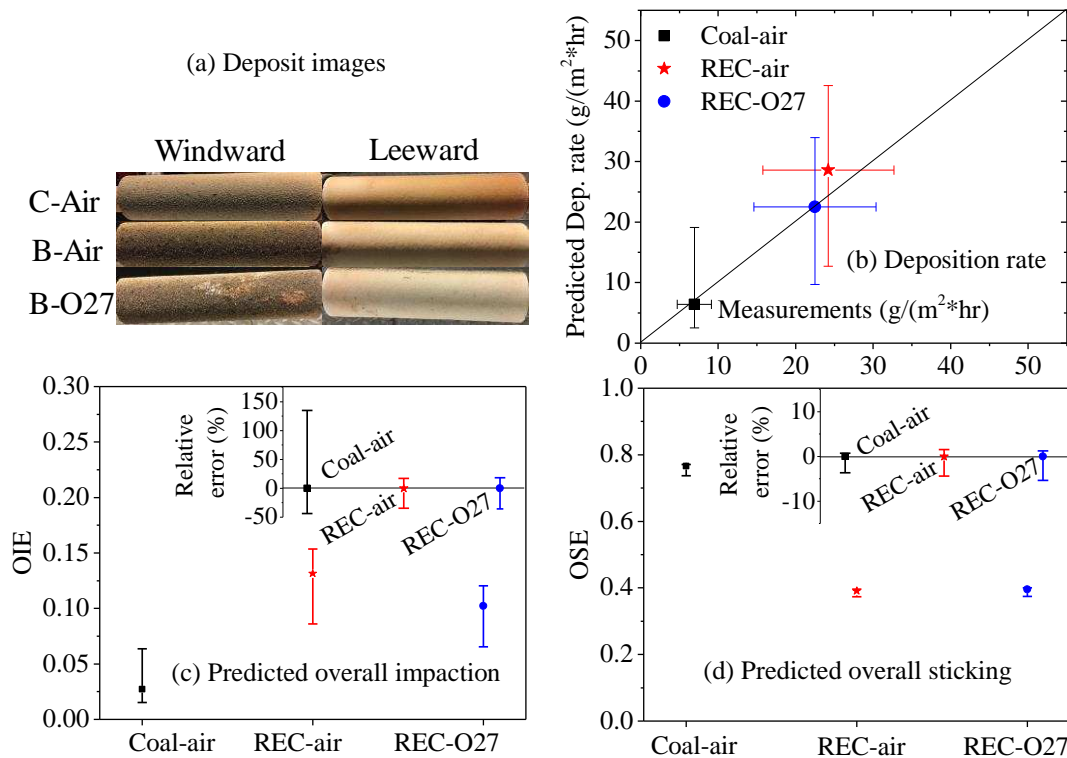
305 sensitivity analysis of $\pm 10\%$ in the average size and -30% in the spreading factor is taken into account by the
306 modelling uncertainty. The second fly ash property is the heterogeneity in the fly ash chemistry, which can affect the
307 particle density and the melting/sticking behaviour. The major mineral species in the fly ash particles from EI
308 Cerrejon coal are SiO_2 (2.65 g/m^3), $\text{CaAl}_2\text{Si}_2\text{O}_8$ (2.73 g/m^3), and Al_2SiO_5 (3.67 g/m^3) while the major species in the
309 fly ash particles from the recycled wood may be SiO_2 (2.65 g/m^3), CaSiO_3 (2.9 g/m^3) and CaO (3.4 g/m^3). Therefore,
310 the possible range of the ash particle density could be $2.65\text{-}3.67 \text{ g/cm}^3$ for coal ash and $2.65\text{-}3.4 \text{ g/cm}^3$ for biomass
311 ash. In addition, with the decrease in the ash particle size, the content in the basic component (e.g., the accumulation
312 of potassium in the fine ash particles due to the vaporisation/agglomeration/condensation [40]) generally increases
313 and the acid component of silicon generally decreases. This may result in the increased melting propensity of the
314 small particles than the large particles. Therefore, a sensitivity analysis of the heterogeneity in the ash chemistry is
315 considered by the assumption of using a particle size dependent particle contact angle: (i) the smallest particle has a
316 relatively low contact angle of 90° (which represents the particle itself being easy to stick) and the largest particle
317 has a relatively high contact angle of 179° (which represents the particle itself being difficult to stick) while the
318 averaged particle had the contact angle of 160° ; (ii) other medium particles are linearly located between these values.
319 Therefore, the combined modelling uncertainties can be determined by the lower bound and upper bound of the
320 uncertainty analysis of the above error sources (the ash content, the particle density, particle size distribution, and the
321 heterogeneity in the ash chemistry), which results in $9 \times 14 = 126$ CFD cases that have been numerically investigated.
322 More details of the model parameters for the uncertainty analysis can be found in the Supplementary Materials.

323 **4 Results and discussion**

324 **4.1 Measured and predicted ash deposition behaviour**

325 Figure 3 shows the measured and predicted ash deposition behaviour. First, the deposit is mainly formed at the
326 windward section of the uncooled tube while there is almost no deposit on the leeward section as shown in Figure
327 3(a). This indicates that both the thermophoretic effect and the eddy impaction are insignificant for the uncooled
328 probe and under a low Reynolds number ($\approx 70\text{-}80$) in the downstream region of the pilot-scale furnace. Second, as
329 shown in Figure 3(b), experimentally, the ash deposition rate for coal air combustion case, $6.9 \text{ g}/(\text{m}^2 \cdot \text{hr})$, is much
330 lower than the recycled wood combustion cases (24.2 and $22.5 \text{ g}/(\text{m}^2 \cdot \text{hr})$ for air and oxyfuel cases, respectively).
331 This is mainly due to the overall particle impaction efficiency for coal, ranging from 1.5% to 6.4% , being much lower
332 than the recycled wood, ranging from 8.6 to 15.4% and 6.6% to 12.1% for air combustion and oxyfuel combustion,
333 respectively, as shown in Figure 3(c). Weber et al. [41] also found that biomass fuels have a much higher deposition

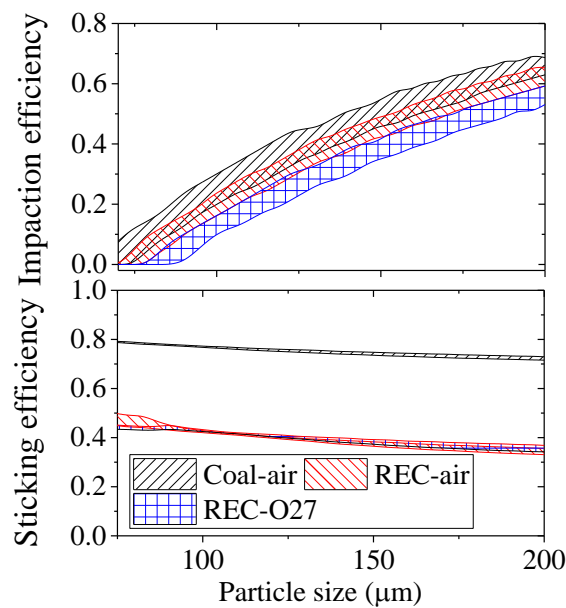
334 rate and particle impaction efficiency than the South African Middleburg coal. However, the predicted impaction
 335 efficiency by Weber et al. [41] is much higher than in the current study. This discrepancy can be attributed to the
 336 particle size of the fly ash being assumed to be constant during combustion process by Weber et al. [41] while the
 337 fly ash size is assumed to be reduced based on the ash content in this study. On the other hand, the overall particle
 338 sticking efficiency for coal has a value of about 0.8, which was approximately twice that of the values (about 0.4) for
 339 biomass. It is interesting that the values of the sticking efficiency in this study are comparable to those presented by
 340 Weber et al. [41], which are approximately 0.8 and 0.4 for the coal and mixed wood under a similar furnace velocity.
 341 In this study, the lower sticking efficiency of the biomass ash particles could be due to the heterogeneity in the fly
 342 ash composition and the larger particle size. For the recycled wood investigated, the main ash composition are silicon
 343 and calcium in the relevant phases. When these two inorganic components separately occur in the fly ash, then they
 344 can be difficult to melt and this can decrease their sticking efficiency. Thirdly, the recycled wood air combustion
 345 case have a slightly lower but similar deposition rate compared to the oxyfuel combustion case since the small
 346 difference in the deposition rate is within the experimental uncertainty. Further, the predicted ash deposition rate has
 347 a similar trend to the measurements, as shown in Figure 3(b).



348
 349 **Figure 3 Measured and predicted ash deposition behaviour ²: (a) Deposit images on the tube; (b)**
 350 **Comparison of the measured and predicted ash deposition rate; (c) Predicted OIE (overall impaction**
 351 **efficiency); (d) Predicted OSE (overall sticking efficiency).**

² Note: (i) The overall impaction efficiency is calculated by the ratio of the overall arrival rate of particles onto the deposition surface to the mass flux of the particles at the projected surface in front of the deposition surface. (ii) The overall sticking efficiency is calculated by the ratio of the deposition rate to the overall arrival rate of the particles onto the

352 Figure 4 shows the predicted ranges for the impaction efficiency and sticking efficiency as a function of particle
 353 size. Interestingly, for size <60-90 μm (correspondingly, particle Stokes numbers were from 0.3-0.5), the particle
 354 impaction efficiency is close to zero. Weber et al. [36] found that the critical particle Stokes number should be
 355 between 0.3-0.4 for Reynolds number between 42.6-106 when only considering the inertia impaction, which is
 356 similar to the current predictions. The particle impaction efficiency gradually increases with the increase in the
 357 particle size (>60-90 μm). This is because, for inertia impaction, smaller particles follow more closely to the fluid
 358 streamlines and they are less likely to impact on the surface, however, the particles with the larger Stokes numbers
 359 are less likely to be affected by the gas flow and more likely to impact on the deposition surface [26, 27]. In addition,
 360 coal and biomass-air cases generally have higher impaction efficiency than the biomass-oxy27 case and this is due
 361 to the decrease in the gas velocity under the oxyfuel combustion condition. In Figure 4, the particle sticking efficiency
 362 generally increases with the reduction in the particle size. In addition, the narrow variations in the predicted particle
 363 sticking efficiency are found and this is due to the impacted particles are coarse particles.



364

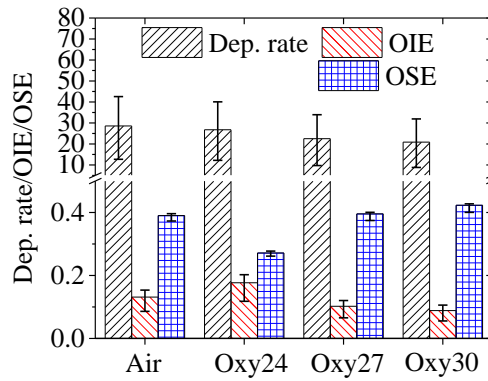
365 **Figure 4 Predicted particle impaction efficiency and sticking efficiency as a function of particle size (the**
 366 **shaded region is the modelling uncertainty).**

367 4.2 The effect of oxyfuel combustion condition

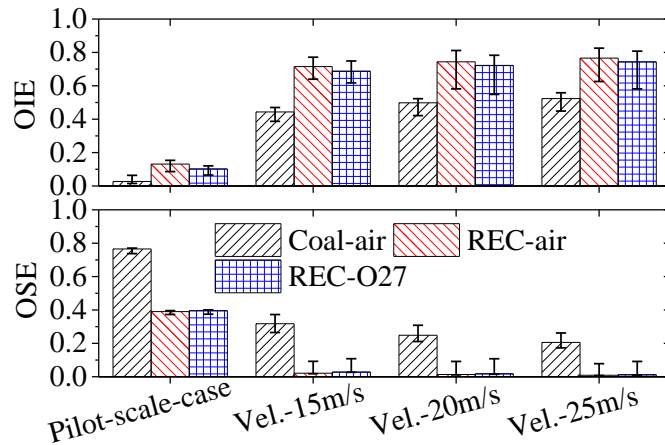
368 Figure 5 shows the effect of the oxyfuel combustion condition (the overall oxygen concentration at the inlets) on
 369 the ash deposit formation. Generally, the predicted ash deposition rates are similar for all cases investigated, but the
 370 oxyfuel cases have slightly lower rates than the air combustion case. The Oxy24 case shows a clear higher overall

deposition surface. (iii) Ash deposition rate is based on the probe area. (iv) The error bars in Figure 3(b) including both the experimental uncertainties and the modelling uncertainties. The other error bars presented in other figures (Figure 3 (c) and (d), Figures 5, 6 and 8) only represent the modelling uncertainties.

371 impaction efficiency and lower sticking efficiency and this is due to the increase in the gas velocity (by 15% compared
 372 to the air combustion case) and decrease in the gas temperature (by 100 °C compared to the air combustion case).
 373 However, the overall particle impaction for the Oxy27 and Oxy30 cases are approximately 20%-30% lower than the
 374 air case while the sticking efficiencies are close to each other. Therefore, this suggests that: (i) When the temperature
 375 profile/heat transfer under oxyfuel conditions are adjusted to match the air conditions, which are similar to the
 376 scenarios for Oxy27 and Oxy30, the slight change in the temperature and velocity does not have a significant
 377 influence on the sticking behaviour; (ii) The change in the gas density and velocity can reduce the particle impaction
 378 efficiency, but the level of the change in the particle impaction behaviour is dictated by the ash size range.

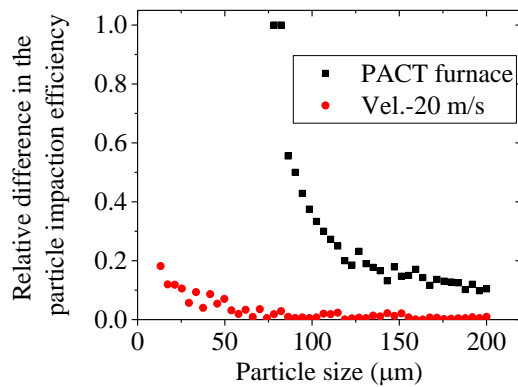


379
 380 **Figure 5 The effect of the oxyfuel combustion condition on the ash deposit formation: (a) Ash deposition rate**
 381 **(g/m²*hr); (b) OIE, Overall impaction efficiency; (c) OSE, Overall sticking efficiency.**



382
 383 **Figure 6 The predicted OIE (overall impaction efficiency) and OSE (overall sticking efficiency) under**
 384 **different flue gas velocity conditions relevant to the boiler conditions³.**

³ Note: the evaluated velocity for the oxy27 cases were assumed to be 20% lower than the air combustion case.



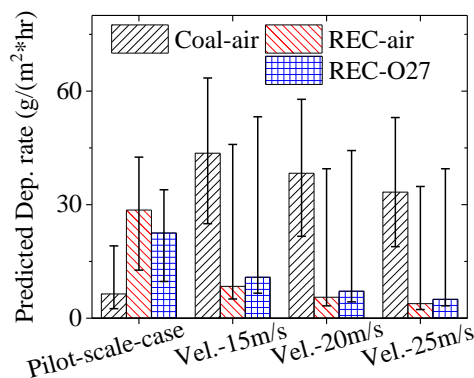
385

386 **Figure 7 The relative difference in the particle impactation efficiency (defined as the ratio of the difference of**
 387 **the impactation efficiency between the air case and the Oxy27 baseline cases to the impactation efficiency of the**
 388 **air case) as a function of particle size.**

389 4.3 The effect of flue gas velocity

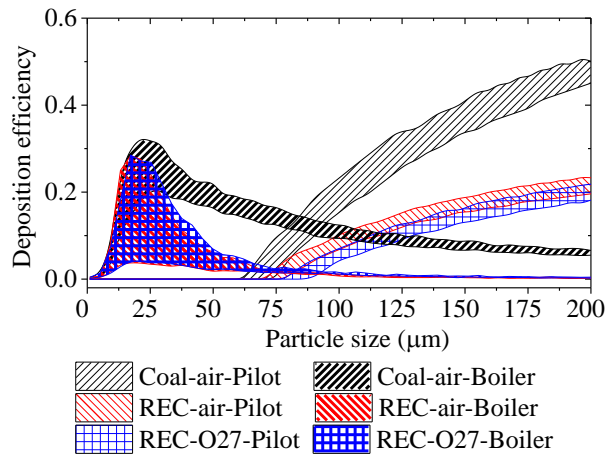
390 The main difference in the furnace conditions between the pilot-scale furnaces and full-scale boilers is the much
 391 lower flue gas velocity in the pilot-scale furnaces [42]. The furnace velocity condition is a significant factor in
 392 dictating the Reynolds number, particle Stokes number and particle kinetic energy. Hence, the change in flue gas
 393 velocity can lead to uncertainties in the ash deposit formation.

394 Figure 6 shows the changes in the overall impactation and sticking behaviours after increasing the flue gas velocity
 395 close to a value used in the boilers. Generally, due to the increase in the particle Stokes number and particle kinetic
 396 energy, the particle impactation efficiency increases from approximately 3% to 50% and 10% to 70% for coal and
 397 biomass, respectively, while the sticking efficiency decreases from 75% to 20% and 40% to 1% for coal and biomass
 398 respectively. Also, under the higher velocities (15-25 m/s), the difference in the particle impactation efficiency between
 399 the air and oxyfuel cases is relatively small, while the difference is much higher for the pilot-scale furnace, as shown
 400 in Figure 7. In the pilot-scale furnace, the effect of the oxyfuel condition on decreasing the impactation efficiency can
 401 effectively increase with the decrease in the particle size. This indicates that the effect can be much larger for fly ash
 402 with a large portion of particles located close to the critical Stokes number.



403

404 **Figure 8 The predicted ash deposition rate under different flue gas velocity conditions relevant to boiler**
 405 **conditions.**



406
 407 **Figure 9 Predicted deposition efficiency as a function of particle size under the gas velocity conditions**
 408 **relevant to the pilot-scale furnace and the velocity being 20 m/s (the shaded region is the modelling**
 409 **uncertainty).**

410 Interestingly, in Figure 8, the predicted ash deposition rate increases from approximately 7 to 30-40 g/m²*hr for
 411 coal while the rate decreases from approximately 25 to 5-10 g/m²*hr for biomass, and this can result in an higher
 412 deposition rate for coal than biomass under the higher velocities. Figure 9 shows the particle size based deposition
 413 efficiency (defined as the impaction efficiency*sticking efficiency)⁴ under the furnace velocity in the pilot-scale
 414 furnace and the velocity being 20 m/s as an example. Interestingly, larger/heavier particles have higher deposition
 415 efficiency in the pilot-scale furnace and the deposition efficiency for particles smaller than the critical Stokes number
 416 was close to zero. This suggests that, due to the low furnace velocity conditions, the pilot-scale furnace favours the
 417 coarse particle deposition and, when only considering the inertia impaction, the pilot-scale furnace can have a ‘cut-
 418 off’ effect for the particles (smaller than the critical Stokes number) on the ash deposit formation. However, after
 419 increasing the velocity to 20 m/s, the highest deposition efficiencies changes from the coarse particles to the fine
 420 particles (approximately 20-30 μm). This suggests that, in the velocity relevant to boiler conditions, the furnace
 421 favours the fine-medium particle deposition.

422 4.4 Discussions

423 4.4.1 Oxyfuel combustion

424 After retrofitting from air combustion to oxyfuel combustion, the reduction in the gas flowrate leads to a decrease
 425 in the flue gas velocity (approximately 20% in this study) and the high concentration of CO₂ increases the gas density
 426 (approximately 40% in this study), which results in the slight increase by approximately 10% in the Reynolds number
 427 and the decrease by approximately 20% and 36% in the particle Stokes number and particle kinetic energy,

⁴ Note: Deposition efficiency represents the possibility of particles being able to deposit. It should be noted that, in addition to deposition efficiency, particle size distribution is the other important factor in dictating the contribution of differently-sized ash particles on deposition.

428 respectively. Therefore, regarding the aerodynamics, the major effects of the oxyfuel combustion on ash deposit
429 formation are mainly caused by the decrease in the particle Stokes number and particle kinetic energy.

430 Under the low velocity condition in the pilot-scale furnace, 20% reduction in the particle Stokes number shows
431 a clear effect on the particle impaction efficiency due to the low Reynolds number (70-80 in this study) and low
432 particle Stokes number (100µm, 0.8-1; 50µm, 0.2-0.3; 10µm, 0.05-0.1 in this study). The degree in the variation of
433 the overall particle impaction efficiency is dictated by the particle size distribution. Generally, with more particles
434 having Stokes number close to the critical Stokes number, $St_{critical}$, the decreased particle impaction efficiency can
435 be larger. When only considering the inertia impaction, the correlation, $St_{critical} = 0.865 * Re^{-0.211}$, is suggested
436 to estimate the critical Stokes number for Reynold numbers ranging from 21.3 to 1065 (suitable for the pilot-scale
437 furnace), derived from the CFD predicted data (critical Stokes number and Reynold number) by Weber et al. [36].
438 On the other hand, the reduction in the particle kinetic energy could not lead to a clear effect on the overall particle
439 sticking behaviour in this study. This may be attributed to the low velocity condition, which results in the particle
440 kinetic energy to be located in the low value region and the predicted particle sticking efficiency is less sensitive to
441 the particle kinetic energy.

442 Under the high velocity condition, which is relevant to full-scale boilers, the reduction in the particle Stokes
443 number does not have an obvious effect on the particle impaction efficiency due to the high Reynolds number (2300-
444 4300 in this study) and high particle Stokes number (100µm, 22-45; 50µm, 5-11; 10µm, 0.2-0.4 in this study). This
445 suggests the change cannot have an obvious effect on the particle impaction behaviour. On the other hand, the
446 decrease in the particle kinetic energy clearly increases the overall particle sticking efficiency by approximately 30%
447 in this study. This may be attributed to the high velocity condition, which results in the predicted particle sticking
448 efficiency being sensitive to the particle kinetic energy.

449 Therefore, this study suggests that: in the pilot-scale furnace, oxyfuel combustion can decrease the particle
450 impaction but the degree in the variation is dictated by the fly ash size distribution; oxyfuel combustion could not
451 have a clear effect on the particle sticking behaviour for the recycled wood, but further studies are needed for more
452 fuels as the particle sticking efficiency is also dictated by the ash chemistry. For retrofitting consideration in boilers,
453 unlike the pilot-scale furnace, oxyfuel combustion cannot effectively decrease the particle impaction efficiency, but
454 the reduction in particle kinetic energy may increase the particle sticking behaviour.

455 4.4.2 From pilot-scale to full-scale

456 The pilot-scale furnace favours the coarse particle deposition due to the low velocity condition while the full-
457 scale furnace favours the deposition of fine-medium particles due to the high velocity condition. When only

458 considering the inertia impaction, the low velocity condition even has a ‘cut-off’ effect on the particle deposition
459 with the particle Stokes number smaller than the critical Stokes number, which does not occur under the high velocity
460 conditions. Therefore, the conclusions of ash deposition behaviours from the pilot-scale furnace cannot be directly
461 employed for the full-scale boilers. In this study, the recycled wood has a much higher deposition rate (three times)
462 than the EI Cerrejon coal in the pilot-scale furnace while the biomass may not be able to have a higher ash deposition
463 rate than the coal when increasing the flue gas velocity conditions to a level in a boiler. Also, the study indicates that
464 solid fuels with a high sticking efficiency (ash contains a large portion of the inorganic species with low melting
465 points) can have a higher deposition rate under the velocities that occur in boilers than the pilot-scale furnace while
466 the solid fuel with a low sticking efficiency (ash contains a large portion of the inorganic species with high melting
467 points) can have an opposite ash deposition behaviour.

468 The study suggests the importance of understanding the detailed fly ash properties (size distribution, size based
469 density, size based ash composition. etc.) to provide a better estimation of the ash deposition propensity in boilers. It
470 is confident to propose that, besides furnace temperature, the aerodynamics and fly ash physicochemical properties
471 can dictate the deposit formation, as shown in Table 3. In the pilot-scale furnace, the fume and fine particles contribute
472 to the deposit formation of the initial layer due to the condensation and the thermophoretic effect, while the coarse
473 and medium particles contribute to the major deposit formation of the other layers. In the boiler, the fume and fine
474 particles contribute to the deposit formation of the initial layer due to the condensation, eddy impaction and the
475 thermophoretic effect, the fine-medium particles contribute to the deposit formation of the other layers, while the
476 coarser particles can not only be more difficult to deposit but also cause erosion and reduce the ash deposit formation.
477 It should be noted that there is a difference in the deposit formation mechanism between slagging and fouling due to
478 the change in the flue gas temperature. For fouling, due to the much lower flue gas temperature, the major ash deposit
479 formation can be dependent on the stickiness of the initial layer of the deposits and the stickiness of the particle
480 surface resulting from the heterogeneous condensed gaseous alkali species. Therefore, the concentrations of the
481 gaseous species and fume particles of potassium/sodium relevant phases are significant in the understanding of the
482 fouling formation and the determining of the solutions to control the fouling issues. For slagging, due to the high flue
483 gas temperature, both the ash particles and the deposit surface are possible to be sticky while the effect of the gaseous
484 alkali species are less important [27]. For woody biomass, potassium and chlorine play a significant contribution in
485 causing serious ash deposit issues due to the low melting temperatures of the potassium related minerals to generate
486 a sticky deposit surface and increase the particle stickiness itself under the pulverised combustion conditions. In
487 addition, high concentrations of potassium in the deposits can increase the degree of sintering [43], which

488 deteriorates the deposit removal. For the recycled woody biomass with a low concentration of potassium used in this
 489 study, the ash deposition should not be serious as both SiO₂ and CaO are less reactive and refractive.

490 **Table 3 Relationship between the particle properties and ash deposit formation for woody biomass (silicon**
 491 **and calcium as the major ash components) in pilot-scale furnaces and full-scale boilers⁵.**

	Particle type	Deposition mechanism	Deposition efficiency	Deposition severity (depending on particle melting potential)
Pilot-scale	Fine particles (fume-submicron sized, micron sized)	Evaporation/nucleation/condensation, Thermophoresis.	Low	Low: SiO ₂ , CaO, Al ₂ O ₃ , etc.; Fe ₂ O ₃ , etc.; High: KCl, K ₂ SO ₄ , etc.;
	Medium (≈ 10-70 μm)	Thermophoresis, Inertia impaction	Low	Low: SiO ₂ , CaO, Al ₂ O ₃ , etc.; Fe ₂ O ₃ , CaSiO ₃ , etc.; High: K ₂ O-SiO ₂ , etc.;
	Coarse (>70 μm)	Inertia impaction	High	Low: SiO ₂ , CaO, Al ₂ O ₃ , etc.; Fe ₂ O ₃ , CaSiO ₃ , etc.; High: K ₂ O-SiO ₂ , etc.;
Full-scale	Fine particles (fume-submicron sized, micron sized)	Evaporation/nucleation/condensation, Thermophoresis, eddy impaction, Inertia impaction (micron sized)	Low	Low: SiO ₂ , CaO, Al ₂ O ₃ , etc.; Fe ₂ O ₃ , etc.; High: KCl, K ₂ SO ₄ , etc.;
	Fine-Medium (≈ 10-70 μm)	Inertia impaction	High	Low: SiO ₂ , CaO, Al ₂ O ₃ , etc.; Fe ₂ O ₃ , CaSiO ₃ , etc.; High: K ₂ O-SiO ₂ , etc.;
	Coarse	Inertia impaction (>70 μm)	Low, or even cause erosion	Low: SiO ₂ , CaO, Al ₂ O ₃ , etc.; Fe ₂ O ₃ , CaSiO ₃ , etc.; High: K ₂ O-SiO ₂ , etc.;

492 4.4.3 Modelling ash deposition

493 An initial uncertainty analysis in the RANS-based CFD modelling of ash deposit formation has been undertaken.
 494 Generally, the experimental measurements, the numerical parameters and the model parameters are considered in
 495 this study. This study suggests that the model parameters relevant to the fly ash formation are the major contributors
 496 to the modelling errors while the uncertainties in the particle tracking can be minimized by using a fine mesh and a
 497 high resolution of the particle size distribution. Fly ash formation dictates the fly ash size distribution, density and
 498 size based ash composition. In this study, the possible range in the size distribution and size based particle sticking

⁵ Trace elements were not discussed in this study for ash deposit formation due to their low concentrations. In addition, the ash composition is represented by the oxides of the ash elements.

499 efficiency might be overestimated since the modelling errors are much larger than the experimental uncertainties,
500 especially for the coal ash deposition case in the pilot-scale furnace and the biomass ash deposition cases under high
501 velocity conditions. A detailed fly ash formation model is urgently needed to better predict the ash deposit formation
502 [29, 44]; alternatively, the experimentally detailed information of the fly ash properties can be used to improve the
503 CFD prediction of the ash deposition. Also, better fly ash properties can be used to accurately derive the particle
504 sticking behaviours from combining the CFD results and experimental measurements [45]. On the other hand, for a
505 cooled heat exchanger tube, dynamic CFD models are required to predict the whole ash deposit formation process
506 [27, 46]. In addition to the uncertainties mentioned above, an uncertainty analysis relevant to the deposit properties
507 (thermal conductivity, porosity, etc.) is needed.

508 **5 Conclusions**

509 (i) Although the recycled wood has a much higher deposition rate than the EI Cerrejon coal in the pilot-scale
510 furnace, the new waste fuel can numerically have a lower deposition rate than the coal under a high velocity condition
511 that is similar those employed in full-scale boilers. This can be due to the much lower sticking efficiency of the
512 recycled wood, which has high concentrations of calcium and silicon, but a low potassium concentration. Ash with
513 a high sticking efficiency can have higher deposition rate under boiler velocity conditions than the pilot-scale ones
514 while ash with a low sticking efficiency can have an opposite trend. In addition, the oxyfuel combustion condition
515 shows a similar deposit formation to the air combustion condition for the recycled wood in both the pilot-scale furnace
516 and the high velocity conditions, where the differences are within the experimental uncertainties.

517 (ii) The effect of oxyfuel combustion condition on ash deposition is different between the pilot-scale furnace and
518 the high velocities in the full-scale boilers. Due to the decrease in the flue gas velocity under oxyfuel condition, both
519 the particle Stokes number and particle kinetic energy can decrease. The decrease in the overall particle impaction
520 efficiency is clearer in the pilot-scale furnace than in the full-scale velocity condition. This is due to the much lower
521 Reynolds number and particle Stokes number in the pilot-scale furnace. Also, the degree of the decrease in the
522 impaction efficiency is dictated by the particle size distribution in the pilot-scale furnace. When there is more ash
523 particles close to the critical Stokes number, the degree of the decrease can be larger. On the other hand, the decrease
524 in the particle kinetic energy has a cleared effect on the increase in the overall particle sticking efficiency in the full-
525 scale velocity conditions than the pilot-scale furnace. This could be due to the much higher velocity and higher
526 particle kinetic energy in the full-scale conditions. However, further studies are required as the particle sticking
527 behaviour is relevant to the ash chemistry as well.

528 (iii) The selective deposition behaviour is different between the pilot-scale furnace and the higher velocity
529 conditions relevant to full-scale boilers. The pilot-scale furnace favours the coarser particle deposition due to the low
530 velocity condition while the full-scale furnace favours the deposition of fine-medium particles due to the high velocity
531 condition. It should be cautious to perform transfer of the deposition observations in the pilot-scale furnace to full-
532 scale boiler. In this study, the predicted ash deposition rate of the recycled wood can be numerically lower than the
533 EI Cerrejon coal when using the full-scale boiler velocity conditions. A relationship between the fly ash particle
534 properties and the deposition propensity for woody biomass is suggested, which is dictated by the aerodynamics and
535 ash physicochemical properties.

536 (iv) The CFD based ash deposition model presents a qualitative agreement with the measurements. An initial
537 modelling uncertainty analysis has been carried out. Uncertainties in the modelling parameters of the fly ash
538 properties (size distribution, size-based ash chemistry, density, etc.) are responsible for the major source of errors
539 along with the possible experimental uncertainties in the fuel analysis of the ash content. The uncertainties in the
540 particle tracking can be minimized by using a fine mesh and high resolution in the particle size distribution.

541 **Acknowledgment**

542 The authors acknowledge the support from the EPSRC grants (EP/M015351/1, Opening New Fuels for UK
543 Generation).

544 **References**

- 545 [1] Chen L, Yong SZ, Ghoniem AF. Oxy-fuel combustion of pulverized coal: Characterization, fundamentals,
546 stabilization and CFD modeling. *Prog Energy Combust* 2012;38(2):156-214.
- 547 [2] Office HMsS. Climate Change Act 2008. Her Majesty's Stationery Office, London, UK; 2008.
- 548 [3] Buhre BJP, Elliott LK, Sheng CD, Gupta RP, Wall TF. Oxy-fuel combustion technology for coal-fired power
549 generation. *Prog Energy Combust* 2005;31(4):283-307.
- 550 [4] Black S, Szuhánszki J, Pranzitelli A, Ma L, Stanger PJ, Ingham DB, et al. Effects of firing coal and biomass under
551 oxy-fuel conditions in a power plant boiler using CFD modelling. *Fuel* 2013;113:780-6.
- 552 [5] Farias Moguel O, Szuhánszki J, Clements AG, Ingham DB, Ma L, Pourkashanian M. Oscillating coal and biomass
553 flames: A spectral and digital imaging approach for air and oxyfuel conditions. *Fuel Process Technol*
554 2018;173:243-52.
- 555 [6] Fryda L, Sobrino C, Cieplik M, van de Kamp WL. Study on ash deposition under oxyfuel combustion of
556 coal/biomass blends. *Fuel* 2010;89(8):1889-902.
- 557 [7] Fryda L, Sobrino C, Glazer M, Bertrand C, Cieplik M. Study of ash deposition during coal combustion under
558 oxyfuel conditions. *Fuel* 2012;92(1):308-17.
- 559 [8] Yu DX, Morris WJ, Erickson R, Wendt JOL, Fry A, Senior CL. Ash and deposit formation from oxy-coal
560 combustion in a 100kW test furnace. *Int J Greenh Gas Con* 2011;5(Supplement 1):S159-S67.
- 561 [9] Li G, Li S, Dong M, Yao Q, Guo CY, Axelbaum RL. Comparison of particulate formation and ash deposition
562 under oxy-fuel and conventional pulverized coal combustions. *Fuel* 2013;106(Supplement C):544-51.
- 563 [10] Brink A, Lindberg D, Hupa M, de Tejada ME, Paneru M, Maier J, et al. A temperature-history based model for
564 the sticking probability of impacting pulverized coal ash particles. *Fuel Process Technol* 2016;141(Part 2):210-5.
- 565 [11] Jurado N, Simms NJ, Anthony EJ, Oakey JE. Effect of co-firing coal and biomass blends on the gaseous
566 environments and ash deposition during pilot-scale oxy-combustion trials. *Fuel* 2017;197:145-58.
- 567 [12] Wu J, Yu D, Liu F, Yu X, Zeng X, Han J, et al. Impact of Oxy-fuel Combustion on Ash Properties and Sintering
568 Strength Development. *Energy Fuels* 2018;32(4):4315-22.

- 569 [13] Yang X, Ingham D, Ma L, Troiano M, Pourkashanian M. Prediction of particle sticking efficiency for fly ash
570 deposition at high temperatures. *Proc Combust Inst* 2019;37(3): 2995-3003.
- 571 [14] Kutchko BG, Kim AG. Fly ash characterization by SEM-EDS. *Fuel* 2006;85(17):2537-44.
- 572 [15] Åmand L-E, Leckner B, Eskilsson D, Tullin C. Ash Deposition on Heat Transfer Tubes during Combustion of
573 Demolition Wood. *Energy Fuels* 2006;20(3):1001-7.
- 574 [16] Vassilev SV, Baxter D, Andersen LK, Vassileva CG. An overview of the composition and application of biomass
575 ash. Part I. Phase-mineral and chemical composition and classification. *Fuel* 2013;105:40-76.
- 576 [17] Vassilev SV, Baxter D, Vassileva CG. An overview of the behaviour of biomass during combustion: Part II. Ash
577 fusion and ash formation mechanisms of biomass types. *Fuel* 2014;117:152-83.
- 578 [18] Näzelius I-L, Boström D, Rebling A, Boman C, Öhman M. Fuel Indices for Estimation of Slagging of
579 Phosphorus-Poor Biomass in Fixed Bed Combustion. *Energy Fuels* 2017;31(1):904-15.
- 580 [19] Boström D, Skoglund N, Grimm A, Boman C, Öhman M, Broström M, et al. Ash Transformation Chemistry
581 during Combustion of Biomass. *Energy Fuels* 2012;26(1):85-93.
- 582 [20] Robinson AL, Junker H, Baxter LL. Pilot-Scale Investigation of the Influence of Coal-Biomass Cofiring on Ash
583 Deposition. *Energy Fuels* 2002;16(2):343-55.
- 584 [21] Birch K, Measurement Good Practice Guide No. 36 – Estimating Uncertainties in Testing, National Physical
585 Laboratory, London, UK, 2001.
- 586 [22] Clements AG, Porter R, Pranzitelli A, Pourkashanian M. Evaluation of FSK models for radiative heat transfer
587 under oxyfuel conditions. *Journal of Quantitative Spectroscopy and Radiative Transfer* 2015;151:67-75.
- 588 [23] Yang X, Clements A, Szuhánszki J, Huang X, Farias Moguel O, Li J, et al. Prediction of the radiative heat transfer
589 in small and large scale oxy-coal furnaces. *Appl Energy* 2018;211:523-37.
- 590 [24] Clements AG, Black S, Szuhánszki J, Stęchly K, Pranzitelli A, Nimmo W, et al. LES and RANS of air and oxy-
591 coal combustion in a pilot-scale facility: Predictions of radiative heat transfer. *Fuel* 2015;151:146-55.
- 592 [25] Yang X, Clements AG, Farias Moguel O, Szuhánszki J, Ma L, Pourkashanian M. CFD modelling of biomass
593 combustion. Sheffield, UK; 2018.
- 594 [26] Yang X, Ingham D, Ma L, Williams A, Pourkashanian M. Predicting ash deposition behaviour for co-combustion
595 of palm kernel with coal based on CFD modelling of particle impaction and sticking. *Fuel* 2016;165:41-9.
- 596 [27] Yang X, Ingham D, Ma L, Zhou H, Pourkashanian M. Understanding the ash deposition formation in Zhundong
597 lignite combustion through dynamic CFD modelling analysis. *Fuel* 2017;194:533-43.
- 598 [28] Ruan R, Tan H, Wang X, Li Y, Li s, Hu Z, et al. Characteristics of fine particulate matter formation during
599 combustion of lignite riched in AAEM (alkali and alkaline earth metals) and sulfur. *Fuel* 2018;211:206-13.
- 600 [29] Kleinhans U, Wieland C, Frandsen FJ, Spliethoff H. Ash formation and deposition in coal and biomass fired
601 combustion systems: Progress and challenges in the field of ash particle sticking and rebound behavior. *Prog
602 Energy Combust* 2018;68:65-168.
- 603 [30] Cai Y, Tay K, Zheng Z, Yang W, Wang H, Zeng G, et al. Modeling of ash formation and deposition processes in
604 coal and biomass fired boilers: A comprehensive review. *Appl Energy* 2018;230:1447-544.
- 605 [31] ANSYS FLUNET 19.2 Theory Guide, ANSYS Inc.
- 606 [32] Chen HC, Patel VC. Near-wall turbulence models for complex flows including separation. *AIAA Journal*
607 1988;26(6):641-8.
- 608 [33] Mills KC, Rhine JM. The measurement and estimation of the physical properties of slags formed during coal
609 gasification: 2. Properties relevant to heat transfer. *Fuel* 1989;68(7):904-10.
- 610 [34] Kupka T, Zając K, Weber R. Effect of Fuel Type and Deposition Surface Temperature on the Growth and
611 Structure of an Ash Deposit Collected during Co-firing of Coal with Sewage Sludge and Sawdust. *Energy & Fuels*
612 2009;23(7):3429-36.
- 613 [35] García Pérez M, Vakkilainen E. A comparison of turbulence models and two and three dimensional meshes for
614 unsteady CFD ash deposition tools. *Fuel* 2019;237:806-11.
- 615 [36] Weber R, Schaffel-Mancini N, Mancini M, Kupka T. Fly ash deposition modelling: Requirements for accurate
616 predictions of particle impaction on tubes using RANS-based computational fluid dynamics. *Fuel* 2013;108:586-
617 96.
- 618 [37] Haugen NEL, Kragset S. Particle impaction on a cylinder in a crossflow as function of Stokes and Reynolds
619 numbers. *J Fluid Mech* 2010;661:239-61.
- 620 [38] Bouhairie S, Chu VH. Two-dimensional simulation of unsteady heat transfer from a circular cylinder in crossflow.
621 *J Fluid Mech* 2007;570:177-215.
- 622 [39] Beckmann AM, Mancini M, Weber R, Seebold S, Müller M. Measurements and CFD modeling of a pulverized
623 coal flame with emphasis on ash deposition. *Fuel* 2016;167:168-79.
- 624 [40] Zhou K, Xu M, Yu D, Liu X, Wen C, Zhan Z, et al. Formation and Control of Fine Potassium-Enriched
625 Particulates during Coal Combustion. *Energy & Fuels* 2010;24(12):6266-74.
- 626 [41] Weber R, Poyraz Y, Beckmann AM, Brinker S. Combustion of biomass in jet flames. *Proceedings of the
627 Combustion Institute* 2015;35(3):2749-58.
- 628 [42] Yang X, Ingham D, Ma L, Srinivasan N, Pourkashanian M. Ash deposition propensity of coals/blends combustion
629 in boilers: a modeling analysis based on multi-slagging routes. *Proc Combust Inst* 2017;36(3):3341-50.
- 630 [43] Wang G, Pinto T, Costa M. Investigation on ash deposit formation during the co-firing of coal with agricultural
631 residues in a large-scale laboratory furnace. *Fuel* 2014;117:269-77.

- 632 [44] Weber R, Mancini M, Schaffel-Mancini N, Kupka T. On predicting the ash behaviour using Computational Fluid
633 Dynamics. *Fuel Process Technol* 2013;105:113-28.
- 634 [45] Huang Q, Li S, Shao Y, Zhao Y, Yao Q. Dynamic evolution of impaction and sticking behaviors of fly ash particle
635 in pulverized coal combustion. *Proc Combust Inst* 2019;37(4):4419-26.
- 636 [46] García Pérez M, Vakkilainen E, Hyppänen T. Fouling growth modeling of kraft recovery boiler fume ash deposits
637 with dynamic meshes and a mechanistic sticking approach. *Fuel* 2016;185:872-85.
638